

Surprised by Attention: Predictable Query Dynamics for Time Series Anomaly Detection

Kadir-Kaan Özer^{1,2}, René Ebeling¹, and Markus Enzweiler²

¹ Mercedes-Benz AG, Germany

{kadir.oezer, rene.ebeling}@mercedes-benz.com

² Institute for Intelligent Systems, Esslingen University of Applied Sciences, Germany
markus.enzweiler@hs-esslingen.de

Abstract. Multivariate time series anomalies often manifest as shifts in cross-channel dependencies rather than simple amplitude excursions. In autonomous driving, for instance, a steering command might be internally consistent but decouple from the resulting lateral acceleration. Residual-based detectors can miss such anomalies when flexible sequence models still reconstruct signals plausibly despite altered coordination.

We introduce **AxonAD**, an unsupervised detector that treats multi-head attention query evolution as a short horizon predictable process. A gradient-updated reconstruction pathway is coupled with a history-only predictor that forecasts future query vectors from past context. This is trained via a masked predictor-target objective against an exponential moving average (EMA) target encoder. At inference, reconstruction error is combined with a tail-aggregated *query mismatch* score, which measures cosine deviation between predicted and target queries on recent timesteps. This dual approach provides sensitivity to structural dependency shifts while retaining amplitude-level detection. On proprietary in-vehicle telemetry with interval annotations and on the TSB-AD multivariate suite (17 datasets, 180 series) with threshold-free and range-aware metrics, AxonAD improves ranking quality and temporal localization over strong baselines. Ablations confirm that query prediction and combined scoring are the primary drivers of the observed gains. Code is available at the URL <https://github.com/iis-esslingen/AxonAD>.

Keywords: Artificial Intelligence · Deep Learning · Machine Learning · Time Series Analysis

1 Introduction

Modern vehicles produce dense telemetry streams where different channels, from steering angle and throttle position to lateral acceleration and yaw rate, are sampled at high frequency. Faults in these systems rarely present as individual channels leaving their nominal range. Instead, the typical failure mode is a *coordination break*: a steering command that no longer produces the expected lateral response, or a throttle position that decouples from engine torque. Detecting

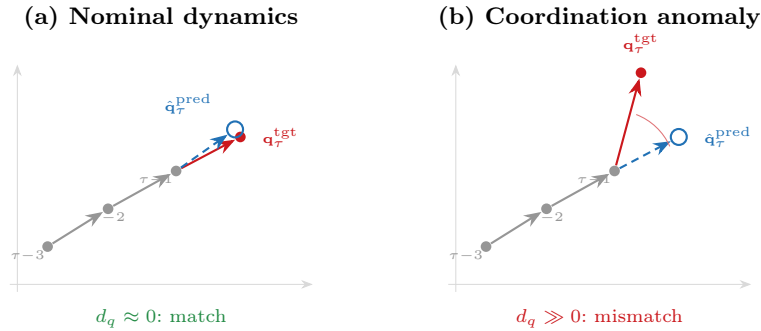


Fig. 1. Query predictability in 2D query space (schematic, single head). Gray: past query trajectory. Blue dashed: predicted query. Red: EMA target query. (a) Nominal: predictor and target agree. (b) Coordination anomaly: the target query diverges from the predicted trajectory, producing large d_q even when per-channel amplitudes are within normal bounds.

such anomalies matters directly for fleet monitoring, warranty analytics, and safety validation.

This setting exposes a fundamental limitation of residual-based unsupervised detectors. A flexible sequence model can accurately reconstruct each channel while missing that the joint coordination pattern across channels has changed [20,28,32]. Low reconstruction error does not guarantee that learned representations preserve the full dependency structure.

Attention mechanisms [30] capture relational structure through query and key matching, but are typically treated as a one-shot computation for the current input window. Under stationary nominal dynamics, the query vectors that control attention routing should evolve predictably over short horizons. Structural anomalies can disrupt this predictability even when per-channel amplitudes remain plausible, making query mismatch a diagnostic signal complementary to reconstruction error. Figure 1 illustrates this idea.

AxonAD combines two coupled pathways. The first reconstructs the input window using bidirectional self attention. The second is a history-only predictor that maps a time-shifted embedding stream to future multi-head query vectors, trained with a masked cosine loss against an exponential moving average (EMA) target encoder. At inference, reconstruction error and query mismatch are each robustly standardized on nominal training data and summed to produce the final anomaly score.

We evaluate on proprietary in-vehicle telemetry with interval annotations as the primary setting and on the multivariate TSB-AD suite [25,22]. Across both, AxonAD improves threshold-free ranking and temporal localization relative to strong baselines, and ablations confirm that query prediction and score combination are the primary drivers.

Our contributions are:

- A predictive attention anomaly detector that treats query vectors as a temporally predictable signal rather than a one-shot routing decision, providing sensitivity to structural dependency shifts.
- Query mismatch as a tail-focused anomaly score that complements reconstruction residuals with a cosine distance signal in query space.
- A stable training scheme based on EMA predictor and target networks with masked supervision, avoiding direct supervision on attention maps or value outputs.

2 Related Work

2.1 Classical Unsupervised Multivariate Detection

Isolation-based methods flag anomalies as points that are easily separated under random partitioning [15,21]. Density and neighborhood methods detect samples whose local geometry differs from the nominal distribution [7,11]. Robust matrix decomposition approaches model data as low-rank structure plus sparse corruption [8], and clustering, histogram, and copula-based methods extend this family with alternative density surrogates [36,16,13,19]. Because none of these methods capture context-dependent coupling that varies across operating modes, they have limited sensitivity to coordination-type anomalies.

2.2 Deep Sequence Models with Residual or Likelihood Scoring

Deep detectors learn nominal dynamics through reconstruction or forecasting and score anomalies by residual magnitude or likelihood deviation. Recurrent reconstruction [24] and probabilistic variants such as VAE and stochastic recurrent models [18,26,27,28,33] perform well across many benchmarks, as do lightweight spectral and convolutional variants [35]. However, residual scoring can miss anomalies that shift dependencies while leaving per-channel values plausible, particularly under nonstationarity where flexible models may still reconstruct accurately despite altered coordination [20,28,32].

2.3 Attention and Relation Aware Anomaly Scoring

Attention weights encode learned relational structure [30] and have been used directly for scoring, for example by measuring association discrepancies [34] or by modeling sensor relations with graph structures [12]. Transformer backbones have also been adapted to anomaly detection through reconstruction and forecasting pipelines [20,29,32,37]. AxonAD differs in that it scores the *predictability* of query vectors over time, capturing what the model is about to attend to, rather than scoring the attention weights themselves or the value residuals.

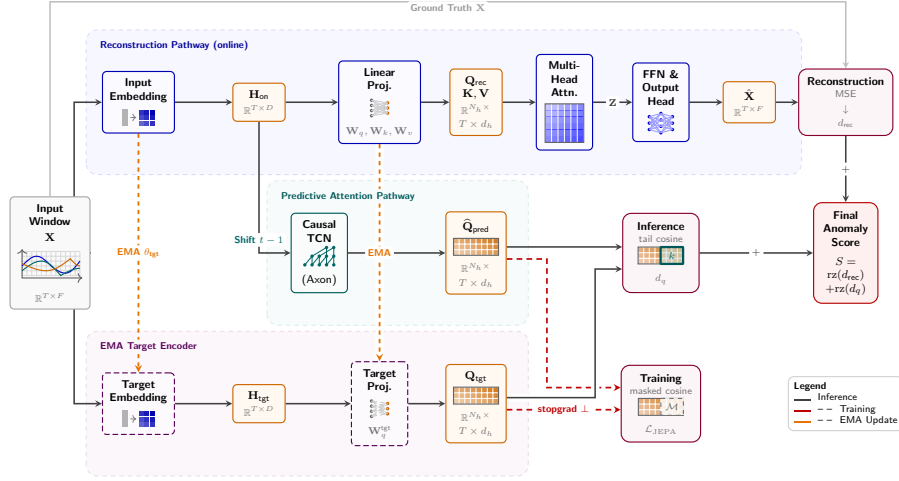


Fig. 2. AxonAD overview. The online reconstruction encoder computes self attention using queries \mathbf{Q}_{rec} . In parallel, a history-only predictor forecasts $\hat{\mathbf{Q}}_{\text{pred}}$ and is trained to match EMA target queries \mathbf{Q}_{tgt} (stop-gradient). Query mismatch on the last valid timesteps yields d_q , and reconstruction yields d_{rec} . Attention divergence (KL tail) is not included in the default scoring pipeline.

2.4 Self-Supervised Predictive Objectives

Predictive self-supervised learning encourages representations to be inferable from context under masking, commonly stabilized via EMA target networks [2,5]. Related masking objectives have been applied to time series representation learning [1,35,37]. Most detectors that use prediction supervise values or latent states and score residuals at inference. AxonAD instead applies predictive supervision directly in query space, making the training objective and the inference scoring signal the same cosine distance. Section 3.4 exploits this consistency.

3 Model Architecture

Figure 2 gives an overview. The model takes a fixed-length window $\mathbf{X} \in \mathbb{R}^{T \times F}$ and produces a reconstruction $\hat{\mathbf{X}} \in \mathbb{R}^{T \times F}$ together with two window-level signals: a reconstruction score d_{rec} and a query mismatch score d_q , combined after robust standardization into the final anomaly score.

The architecture has three components: (i) a gradient-updated reconstruction pathway based on bidirectional self attention, (ii) a history-only predictive pathway that forecasts future multi-head query vectors from a time-shifted embedding stream, and (iii) an EMA target encoder that provides stable query supervision targets [14]. Throughout this paper, *online* refers to gradient-updated parameters, not streaming causality.

Notation. T denotes the window length, F the number of channels, and D the embedding dimension. N_h is the number of attention heads with head dimension $d_h = D/N_h$. s is the forecast horizon, k the number of tail timesteps used for query mismatch aggregation, and $m \in (0, 1)$ is the EMA momentum. We use $\tau \in \{1, \dots, T\}$ for within window timestep indices. For a window ending at absolute time t , we write $\mathbf{X}_{t-T+1:t} \in \mathbb{R}^{T \times F}$ for its T rows.

Shared embedding. A linear projection with learnable positional bias maps \mathbf{X} to a shared per timestep representation, followed by layer normalization [4] applied before attention:

$$\mathbf{H}_{\text{on}} = \text{LN}(\mathbf{X}\mathbf{W}_e + \mathbf{b}_e + \mathbf{P}), \quad \mathbf{P} \in \mathbb{R}^{T \times D}.$$

This sequence feeds both the reconstruction self attention and the predictive branch (after applying the history-only time shift described below).

3.1 Online Reconstruction Pathway

The online encoder forms multi-head queries, keys, and values via learned projections:

$$(\mathbf{Q}_{\text{rec}}, \mathbf{K}, \mathbf{V}) \in \mathbb{R}^{N_h \times T \times d_h}.$$

Standard multi-head self attention [30] over full within window context produces context features \mathbf{Z} , which are processed by a position-wise feedforward network and a linear output head to obtain $\hat{\mathbf{X}}$. The reconstruction score is the mean squared ℓ_2 error over timesteps:

$$d_{\text{rec}} = \frac{1}{T} \sum_{\tau=1}^T \|\hat{\mathbf{x}}_{\tau} - \mathbf{x}_{\tau}\|_2^2. \quad (1)$$

3.2 Predictive Attention Pathway

The predictive pathway forecasts query vector evolution using only past context, producing an anomaly signal sensitive to coordination shifts even when windows remain plausible in amplitude.

History-only shift. To prevent information leakage, we construct a time-shifted embedding stream with forecast horizon s :

$$\tilde{\mathbf{H}}_{\tau} = \begin{cases} \mathbf{0}, & \tau \leq s, \\ \mathbf{H}_{\text{on}, \tau-s}, & \tau > s, \end{cases}$$

ensuring that any prediction at timestep τ depends only on embeddings available up to $\tau - s$.

Causal predictor. A causal temporal predictor $g(\cdot)$ maps the shifted sequence to predicted multi-head queries:

$$\hat{\mathbf{Q}}_{\text{pred}} = g(\tilde{\mathbf{H}}) \in \mathbb{R}^{N_h \times T \times d_h},$$

with causality enforced so that the output at τ depends only on $\tilde{\mathbf{H}}_{\leq\tau}$. We denote the per head, per timestep slice by $\hat{\mathbf{q}}_{h,\tau}^{\text{pred}} = \hat{\mathbf{Q}}_{\text{pred}}[h, \tau, :] \in \mathbb{R}^{d_h}$, with the corresponding EMA target slice $\mathbf{q}_{h,\tau}^{\text{tgt}}$ defined in Section 3.3. The predictive branch forecasts queries only, not keys or values, keeping it lightweight and aligning supervision directly with the inference scoring signal.

3.3 EMA Target Encoder and Masked Training

We maintain an EMA target encoder with parameters θ_{tgt} that track the online parameters θ_{on} :

$$\theta_{\text{tgt}} \leftarrow m \theta_{\text{tgt}} + (1 - m) \theta_{\text{on}}, \quad m \in (0, 1),$$

with no gradient updates to the target parameters [14]. Given the same input window \mathbf{X} , the EMA encoder produces a target embedding sequence $\mathbf{H}_{\text{tgt}} \in \mathbb{R}^{T \times D}$ in the same way as \mathbf{H}_{on} but using θ_{tgt} . Target queries are obtained via a mirrored projection:

$$\mathbf{Q}_{\text{tgt}} = \text{reshape}_{N_h}(\mathbf{H}_{\text{tgt}} \mathbf{W}_q^{\text{tgt}}) \in \mathbb{R}^{N_h \times T \times d_h}, \quad (2)$$

where $\mathbf{W}_q^{\text{tgt}}$ is the EMA tracked counterpart of the online query projection.

Training minimizes reconstruction error together with a masked cosine loss in query space, following a JEPA style scheme [2]. A set of masked timesteps $\mathcal{M} \subset \{s + 1, \dots, T\}$ is sampled via contiguous time patch masking over valid timesteps (inputs remain unmasked). The resulting loss is:

$$\mathcal{L}_{\text{JEPA}} = \frac{1}{|\mathcal{M}| N_h} \sum_{\tau \in \mathcal{M}} \sum_{h=1}^{N_h} \left(1 - \left\langle \frac{\hat{\mathbf{q}}_{h,\tau}^{\text{pred}}}{\|\hat{\mathbf{q}}_{h,\tau}^{\text{pred}}\|_2 + \varepsilon_{\text{cos}}}, \frac{\text{stopgrad}(\mathbf{q}_{h,\tau}^{\text{tgt}})}{\|\text{stopgrad}(\mathbf{q}_{h,\tau}^{\text{tgt}})\|_2 + \varepsilon_{\text{cos}}} \right\rangle \right). \quad (3)$$

The stop-gradient on $\mathbf{q}_{h,\tau}^{\text{tgt}}$ ensures that only the predictor is updated to match the targets, not the reverse.

3.4 Query Mismatch and Final Anomaly Score

At inference, AxonAD computes two complementary window-level signals: d_{rec} (Eq. (1)) and a query mismatch score d_q derived from cosine deviations between predicted and EMA target queries on the *tail* of the window, emphasizing the most recent timesteps.

The tail-aggregated query mismatch is defined as:

$$\begin{aligned} \tau_0 &= \max(s + 1, T - k + 1), \\ k_{\text{eff}} &= T - \tau_0 + 1, \\ d_q &= \frac{1}{N_h k_{\text{eff}}} \sum_{h=1}^{N_h} \sum_{\tau=\tau_0}^T \left(1 - \left\langle \frac{\hat{\mathbf{q}}_{h,\tau}^{\text{pred}}}{\|\hat{\mathbf{q}}_{h,\tau}^{\text{pred}}\|_2 + \varepsilon_{\text{cos}}}, \frac{\mathbf{q}_{h,\tau}^{\text{tgt}}}{\|\mathbf{q}_{h,\tau}^{\text{tgt}}\|_2 + \varepsilon_{\text{cos}}} \right\rangle \right), \end{aligned} \quad (4)$$

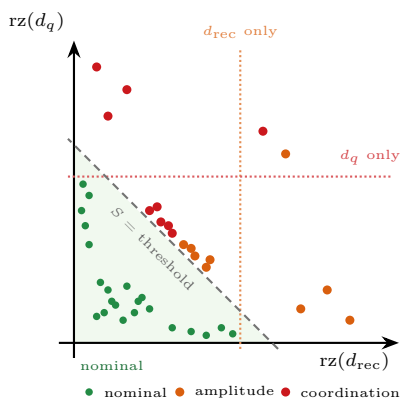


Fig. 3. Score complementarity (schematic). **Nominal** windows spread along both axes but cluster near the origin in both scores simultaneously. Near-boundary **amplitude** and **coordination** anomalies are moderate on both axes, falling inside both single-axis thresholds (dotted lines) but separated by the additive S (dashed diagonal).

where τ_0 enforces both validity under the s step history constraint and tail focus of nominal length k , and k_{eff} normalizes by the actual number of summed timesteps.

Because d_{rec} and d_q can have very different dynamic ranges across datasets, each component is robustly standardized using median and interquartile range (IQR) statistics computed exclusively on nominal training windows:

$$\text{rz}(u) = \frac{u - \text{median}(u)}{\text{IQR}(u) + \varepsilon_{\text{rz}}}, \quad \text{IQR}(u) = Q_{0.75}(u) - Q_{0.25}(u), \quad (5)$$

and the final anomaly score is:

$$S(\mathbf{X}) = \text{rz}(d_{\text{rec}}(\mathbf{X})) + \text{rz}(d_q(\mathbf{X})). \quad (6)$$

The additive form means that a single threshold on S captures anomalies that elevate either component or both. Figure 3 illustrates the geometry: amplitude anomalies raise d_{rec} while coordination anomalies raise d_q , and the diagonal constant score contour separates all anomaly types from the nominal cluster.

Training and inference consistency. The cosine distance used for masked supervision in Eq. (3) is the same metric reused at inference as d_q in Eq. (4). This means the predictor is trained directly on the deployed scoring objective. An attention divergence diagnostic (KL tail) is implemented for ablation analysis only and is not part of the default scoring pipeline.

4 Experimental Setup

Protocol. We evaluate in two settings: (i) proprietary in-vehicle telemetry with interval annotations, and (ii) the TSB-AD multivariate suite (17 datasets,

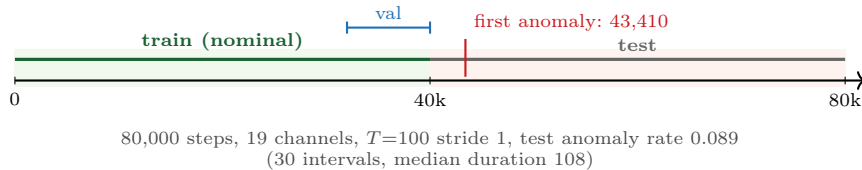


Fig. 4. Chronological split and anomaly onset for the proprietary telemetry stream.

180 series) under the official pipeline [22,25]. Training is strictly unsupervised. All parameters and robust scoring statistics are fit on nominal training windows only, with labels reserved for evaluation. Hyperparameters for all methods are selected on the official TSB-AD tuning component (20 multivariate series) and then fixed. Telemetry labels are never used for hyperparameter selection, thresholding, postprocessing, or early stopping. Early stopping uses a fixed criterion (validation reconstruction error) on an unlabeled split carved from the nominal training prefix.

Label-free transfer check. To verify that hyperparameters selected on TSB-AD transfer reasonably to the telemetry domain, we compare distributional similarity using z-scored summary features (scale, shape, autocorrelation, and spectral descriptors) computed on train segments. The telemetry segment is not an outlier: its leave-one-out Mahalanobis distance falls at the 45th percentile and its nearest-neighbor distance at the 55th percentile.

4.1 Datasets, Splits, and Windowing

The proprietary telemetry stream contains 80,000 timesteps with $F=19$ continuous channels (Figure 4). Anomalies are annotated as contiguous intervals (30 total, duration 1 to 292 with median 108, affecting 1 to 4 channels with median 2) spanning the following types: flatline, drift, level shift, spike, variance jump, and correlation break. The chronological split is: train $[0, 40000)$ with an internal 20% validation holdout (train_sub $[0, 32000)$, val $[32000, 40000)$), and test $[40000, 80000)$. The first anomaly occurs at index 43,410, so both training and validation partitions are anomaly free.

The TSB-AD multivariate suite aggregates 180 series across 17 datasets [25,22]. We follow the official evaluator and protocol throughout.

Causality and latency. Window scoring uses no lookahead: $S(\mathbf{X}_{t-T+1:t})$ depends only on samples up to t . For real-time deployment, each window score is naturally assigned to its endpoint t (detection time). However, to comply with the point-wise metric computation of the TSB-AD evaluation framework, offline benchmark scores are assigned to the center of the window at $t - \lfloor (T-1)/2 \rfloor$. This sequence alignment applies boundary edge padding and effectively incorporates a lookahead of $\lfloor (T-1)/2 \rfloor$ steps solely for temporal localization evaluation. Reconstruction attention remains bidirectional within each window, while query prediction is history-only via the s step shift.

4.2 Baselines and Metrics

We compare against classical, deep reconstruction and forecasting, and Transformer-based detectors implemented in the official TSB-AD framework: Isolation Forest [21], Extended Isolation Forest [15], LSTMAD [24], OmniAnomaly [28], USAD [3], VAE variants [10,18,26,27] including VASP [31], and Transformer-based baselines (TFTResidual [20], TimesNet [32], TranAD [29], Anomaly Transformer [34]). The main paper reports a representative subset, with full results in the Appendix.

We report threshold-free ranking via AUC-ROC, AUC-PR, VUS-ROC, and VUS-PR [6], and localization via PA-F1, Event-F1, Range-F1, and Affiliation-F1 using the official evaluator [22,25]. For F1 family metrics, operating points follow the evaluator’s default threshold sweep (oracle).

4.3 AxonAD Configuration

A single configuration is used across all datasets. The model applies a linear embedding with learnable positional bias ($\mathcal{N}(0, 0.02)$), prenorm multi-head self attention, and a feedforward network of width $2D$ with ReLU. The predictive branch is a causal temporal convolutional network [17] with dilations (1, 2, 4, 8), kernel size 3, and dropout 0.1. The EMA target encoder [14] is initialized from the online model and updated each step with momentum $m=0.9$. Query supervision uses time patch masking focused on later timesteps (mask ratio 0.5, block fraction 0.5). Training minimizes reconstruction MSE plus cosine query prediction loss with uncertainty weighting [9], optimized via AdamW [23] (weight decay 10^{-5}), gradient clipping at 1.0, and early stopping on validation reconstruction error.

Unless stated otherwise, reported results use $T=100$, $D=128$, 8 attention heads, forecast horizon $s=1$, tail length $k=10$, learning rate 5×10^{-4} , batch size 128, and up to 50 epochs with patience 3. Results are averaged over four seeds {2024, . . . , 2027}. All experiments have been run on a single Apple MacBook Pro (M3 Max, 32 GB unified memory) using PyTorch with Apple Silicon acceleration.

5 Results

We first report results on the proprietary telemetry stream, which is the primary applied setting, and then on the TSB-AD benchmark to assess generalization.

Table 1 reports results on the proprietary telemetry stream. AxonAD achieves the strongest threshold-free metrics by a wide margin, with AUC-PR of 0.285 versus 0.128 for the next best method (SISVAE). The gains are especially pronounced on Event-F1 (0.420 vs 0.255) and Range-F1 (0.328 vs 0.262), indicating that AxonAD not only ranks anomalies more accurately but also localizes them better in time. The large gap is consistent with the prevalence of coordination breaks in this dataset: anomalies that alter cross-channel dependencies without producing large per-channel excursions are precisely the regime where query mismatch provides the most value.

Table 1. Proprietary telemetry results (TSB-AD evaluation suite). Mean \pm std over four seeds. Best per metric in **bold**.

Model	Proprietary Telemetry (19 channels, 80,000 timesteps)							
	AUC-PR	AUC-ROC	VUS-PR	VUS-ROC	PA-F1	Event-F1	Range-F1	Affiliation-F1
LSTMAD [24]	0.082 \pm 0.004	0.651 \pm 0.009	0.083 \pm 0.004	0.624 \pm 0.009	0.533 \pm 0.014	0.255 \pm 0.015	0.139 \pm 0.006	0.723 \pm 0.003
SISVAE [18]	0.128 \pm 0.030	0.586 \pm 0.026	0.070 \pm 0.012	0.504 \pm 0.052	0.270 \pm 0.100	0.231 \pm 0.060	0.225 \pm 0.054	0.699 \pm 0.018
TFTRResidual [20]	0.071 \pm 0.006	0.644 \pm 0.025	0.070 \pm 0.005	0.582 \pm 0.018	0.424 \pm 0.022	0.164 \pm 0.019	0.110 \pm 0.009	0.752 \pm 0.026
VSVAE [26]	0.100 \pm 0.005	0.617 \pm 0.031	0.065 \pm 0.005	0.535 \pm 0.027	0.214 \pm 0.048	0.188 \pm 0.004	0.262 \pm 0.037	0.730 \pm 0.012
M2N2 [1]	0.065 \pm 0.001	0.596 \pm 0.001	0.064 \pm 0.001	0.553 \pm 0.004	0.392 \pm 0.022	0.196 \pm 0.020	0.120 \pm 0.009	0.680 \pm 0.000
MAVAE [10]	0.094 \pm 0.006	0.561 \pm 0.034	0.059 \pm 0.006	0.487 \pm 0.051	0.220 \pm 0.076	0.199 \pm 0.015	0.202 \pm 0.017	0.680 \pm 0.000
VASP [31]	0.050 \pm 0.001	0.540 \pm 0.014	0.051 \pm 0.002	0.449 \pm 0.016	0.190 \pm 0.008	0.099 \pm 0.004	0.119 \pm 0.013	0.686 \pm 0.008
WVAE [27]	0.087 \pm 0.013	0.541 \pm 0.043	0.057 \pm 0.007	0.467 \pm 0.050	0.249 \pm 0.103	0.226 \pm 0.038	0.163 \pm 0.011	0.680 \pm 0.000
TimesNet [32]	0.055 \pm 0.001	0.579 \pm 0.003	0.056 \pm 0.000	0.531 \pm 0.003	0.306 \pm 0.020	0.102 \pm 0.004	0.092 \pm 0.002	0.680 \pm 0.000
IForest [21]	0.041 \pm 0.000	0.472 \pm 0.000	0.044 \pm 0.000	0.328 \pm 0.000	0.140 \pm 0.000	0.086 \pm 0.000	0.195 \pm 0.000	0.682 \pm 0.000
TranAD [29]	0.041 \pm 0.000	0.470 \pm 0.003	0.044 \pm 0.000	0.417 \pm 0.004	0.237 \pm 0.003	0.086 \pm 0.000	0.107 \pm 0.007	0.680 \pm 0.000
USAD [3]	0.040 \pm 0.001	0.470 \pm 0.010	0.044 \pm 0.001	0.371 \pm 0.011	0.122 \pm 0.005	0.087 \pm 0.001	0.152 \pm 0.033	0.682 \pm 0.001
OmniAnomaly [28]	0.041 \pm 0.000	0.459 \pm 0.000	0.043 \pm 0.000	0.338 \pm 0.000	0.150 \pm 0.000	0.086 \pm 0.000	0.126 \pm 0.000	0.680 \pm 0.000
AxonAD (ours)	0.285 \pm 0.014	0.702 \pm 0.011	0.157 \pm 0.012	0.634 \pm 0.017	0.533 \pm 0.016	0.420 \pm 0.019	0.328 \pm 0.014	0.715 \pm 0.024

Table 2. TSB-AD multivariate benchmark (17 datasets, 180 series). Mean \pm std over all series. Best per metric in **bold**.

Model	TSB-AD (multivariate, 17 datasets, 180 time series)							
	AUC-PR	AUC-ROC	VUS-PR	VUS-ROC	PA-F1	Event-F1	Range-F1	Affiliation-F1
VASP [31]	0.339 \pm 0.319	0.762 \pm 0.195	0.401 \pm 0.338	0.809 \pm 0.185	0.669 \pm 0.318	0.520 \pm 0.361	0.400 \pm 0.260	0.849 \pm 0.123
OmniAnomaly [28]	0.372 \pm 0.341	0.744 \pm 0.250	0.424 \pm 0.354	0.777 \pm 0.240	0.627 \pm 0.354	0.528 \pm 0.367	0.432 \pm 0.292	0.841 \pm 0.126
WVAE [27]	0.354 \pm 0.331	0.747 \pm 0.248	0.413 \pm 0.349	0.778 \pm 0.248	0.576 \pm 0.388	0.502 \pm 0.383	0.365 \pm 0.280	0.838 \pm 0.137
USAD [3]	0.363 \pm 0.339	0.738 \pm 0.256	0.412 \pm 0.350	0.771 \pm 0.244	0.622 \pm 0.355	0.519 \pm 0.364	0.422 \pm 0.288	0.837 \pm 0.131
SISVAE [18]	0.323 \pm 0.290	0.759 \pm 0.234	0.372 \pm 0.315	0.786 \pm 0.227	0.551 \pm 0.367	0.470 \pm 0.355	0.369 \pm 0.278	0.824 \pm 0.129
MAVAE [10]	0.299 \pm 0.297	0.697 \pm 0.256	0.351 \pm 0.322	0.728 \pm 0.256	0.568 \pm 0.372	0.463 \pm 0.360	0.325 \pm 0.264	0.812 \pm 0.132
VSVAE [26]	0.290 \pm 0.286	0.709 \pm 0.256	0.342 \pm 0.321	0.734 \pm 0.257	0.596 \pm 0.355	0.487 \pm 0.347	0.374 \pm 0.254	0.841 \pm 0.121
M2N2 [1]	0.319 \pm 0.358	0.740 \pm 0.198	0.323 \pm 0.359	0.779 \pm 0.183	0.876 \pm 0.184	0.603 \pm 0.372	0.282 \pm 0.233	0.860 \pm 0.118
TranAD [29]	0.258 \pm 0.318	0.675 \pm 0.221	0.308 \pm 0.347	0.742 \pm 0.210	0.753 \pm 0.314	0.530 \pm 0.367	0.218 \pm 0.154	0.826 \pm 0.125
TFTRResidual [20]	0.250 \pm 0.313	0.710 \pm 0.210	0.308 \pm 0.338	0.777 \pm 0.186	0.746 \pm 0.318	0.472 \pm 0.362	0.207 \pm 0.161	0.846 \pm 0.114
TimesNet [32]	0.201 \pm 0.246	0.618 \pm 0.279	0.271 \pm 0.297	0.686 \pm 0.277	0.750 \pm 0.292	0.427 \pm 0.354	0.176 \pm 0.129	0.821 \pm 0.117
IForest [21]	0.210 \pm 0.232	0.704 \pm 0.191	0.253 \pm 0.260	0.750 \pm 0.184	0.655 \pm 0.335	0.403 \pm 0.322	0.243 \pm 0.178	0.801 \pm 0.110
LSTMAD [24]	0.248 \pm 0.328	0.597 \pm 0.337	0.245 \pm 0.329	0.626 \pm 0.343	0.657 \pm 0.412	0.507 \pm 0.413	0.198 \pm 0.175	0.701 \pm 0.350
AxonAD (ours)	0.437 \pm 0.323	0.825 \pm 0.169	0.493 \pm 0.325	0.859 \pm 0.146	0.698 \pm 0.316	0.600 \pm 0.336	0.471 \pm 0.290	0.860 \pm 0.132

Table 1 shows that these gains generalize beyond telemetry. On the TSB-AD multivariate suite, AxonAD achieves the highest mean AUC-PR (0.437), VUS-PR (0.493), and Range-F1 (0.471). M2N2 leads on PA-F1, and VASP and OmniAnomaly are competitive on Affiliation-F1, but all three rank below AxonAD on threshold-free metrics. Classical detectors achieve moderate AUC-ROC but lower AUC-PR and range-aware scores. Transformer-based detectors are competitive on subsets of series but show lower mean ranking in aggregate.

Figure 5 confirms that improvements are broadly distributed: AxonAD wins on a clear majority of the 180 series against every baseline, with all paired Wilcoxon signed-rank tests yielding $p < 10^{-4}$.

6 Ablation Studies

Table 3 reports ablations on the TSB-AD multivariate tuning subset (20 series) under the official protocol. All variants share identical preprocessing, windowing, and metric computation. Rows are grouped by the design dimension under study and discussed in that order below.

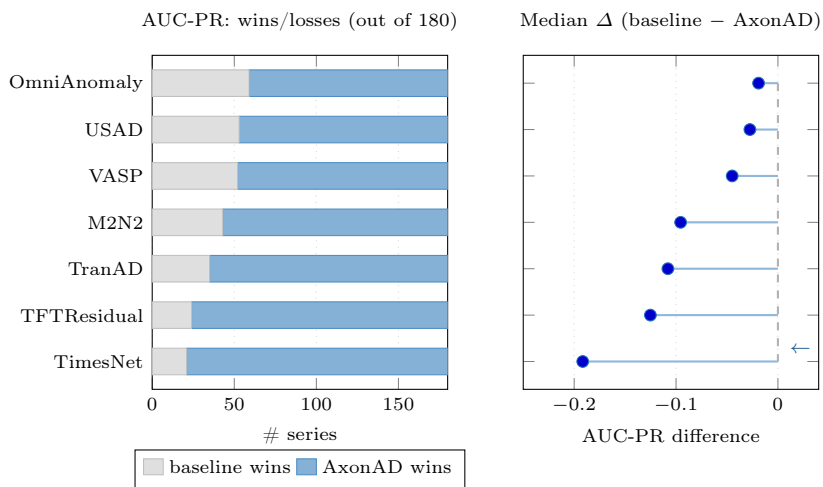


Fig. 5. Paired AUC-PR comparison on TSB-AD multivariate ($n = 180$). Left: win/loss counts. Right: median paired difference with lollipop connectors from zero. All paired Wilcoxon tests yield $p < 10^{-4}$ with entirely negative 95% bootstrap CIs (full statistics in the Appendix).

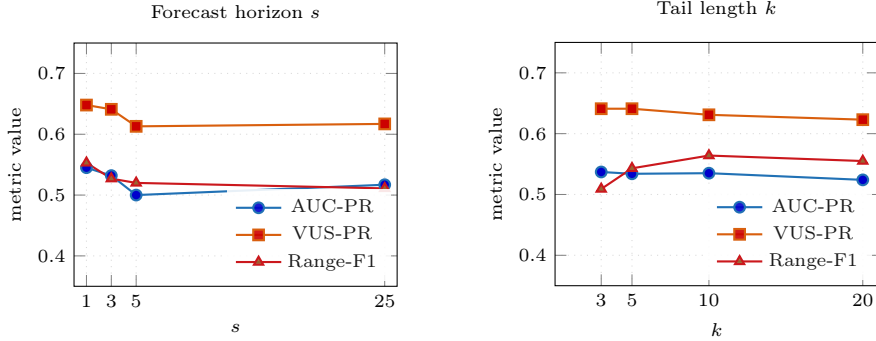
Scoring components. The base configuration (*Base*) achieves the strongest balanced profile across ranking and localization metrics. Removing the query branch at inference and using $S = rz(d_{\text{rec}})$ alone (*Recon only*) reduces VUS-PR by 0.055 and Event-F1 by 0.117. Retaining both branches but replacing cosine mismatch with MSE distance in query space (*Score MSE*) yields a similar drop, indicating that the cosine formulation matters beyond simply combining two scores. Using the query signal alone (*JEPA only, Q*) reduces AUC-PR by 0.145 and AUC-ROC by 0.097 despite retaining competitive PA-F1, confirming that reconstruction is necessary for reliable ranking across all anomaly types. The cosine-based combined score therefore yields the most reliable behavior across metric families.

KL tail. Adding attention divergence on top of the default score (*Score MSE+JEPA KL*) yields no consistent improvement over *Base* on any metric. We treat the KL tail as a diagnostic signal only and exclude it from the default scoring pipeline.

EMA and masking. Removing the EMA target encoder entirely (*EMA 0*, i.e. $m = 0$) reduces AUC-PR by 0.024 and Event-F1 by 0.051. Moderate momentum (*EMA 0.99*, $m = 0.99$) incurs a similar AUC-PR penalty of 0.048, while very high momentum (*EMA 0.999*, $m = 0.999$) likewise degrades ranking; both extremes confirm that the default $m = 0.9$ strikes the right balance between target stability and responsiveness to online updates. Increasing the masking ratio to 0.8 (*Mask 0.8*) similarly reduces AUC-PR and Event-F1, indicating that overly aggressive masking makes the predictive task too hard during training.

Table 3. AxonAD ablation on the TSB-AD multivariate tuning subset (20 series). Mean \pm std. Best per metric in **bold**. Rows are grouped to match the discussion order below.

Variant	TSB-AD (multivariate, ablation subset)							
	AUC-PR	AUC-ROC	VUS-PR	VUS-ROC	PA-F1	Event-F1	Range-F1	Affiliation-F1
Base	0.558 \pm 0.285	0.861 \pm 0.137	0.658 \pm 0.301	0.915 \pm 0.102	0.855 \pm 0.248	0.773 \pm 0.262	0.564 \pm 0.263	0.904 \pm 0.123
Recon only	0.511 \pm 0.330	0.820 \pm 0.218	0.603 \pm 0.366	0.858 \pm 0.223	0.728 \pm 0.325	0.656 \pm 0.322	0.541 \pm 0.303	0.856 \pm 0.142
Score MSE	0.513 \pm 0.327	0.828 \pm 0.204	0.604 \pm 0.365	0.868 \pm 0.208	0.730 \pm 0.317	0.652 \pm 0.311	0.534 \pm 0.293	0.852 \pm 0.139
JEPA only, Q	0.413 \pm 0.317	0.764 \pm 0.200	0.533 \pm 0.353	0.846 \pm 0.177	0.822 \pm 0.283	0.683 \pm 0.321	0.396 \pm 0.248	0.892 \pm 0.114
Score MSE+JEPA KL	0.554 \pm 0.285	0.860 \pm 0.137	0.655 \pm 0.300	0.916 \pm 0.100	0.854 \pm 0.248	0.772 \pm 0.262	0.560 \pm 0.266	0.896 \pm 0.127
EMA 0	0.534 \pm 0.302	0.855 \pm 0.143	0.636 \pm 0.319	0.908 \pm 0.113	0.818 \pm 0.250	0.722 \pm 0.266	0.560 \pm 0.258	0.873 \pm 0.134
EMA 0.99	0.510 \pm 0.325	0.859 \pm 0.137	0.608 \pm 0.350	0.910 \pm 0.105	0.824 \pm 0.246	0.700 \pm 0.269	0.564 \pm 0.263	0.883 \pm 0.127
EMA 0.999	0.527 \pm 0.310	0.856 \pm 0.146	0.636 \pm 0.322	0.913 \pm 0.114	0.804 \pm 0.249	0.724 \pm 0.269	0.556 \pm 0.261	0.882 \pm 0.134
Mask 0.8	0.533 \pm 0.306	0.859 \pm 0.142	0.631 \pm 0.329	0.911 \pm 0.111	0.808 \pm 0.251	0.703 \pm 0.271	0.547 \pm 0.263	0.864 \pm 0.137
Heads=4	0.525 \pm 0.306	0.856 \pm 0.139	0.630 \pm 0.323	0.914 \pm 0.101	0.808 \pm 0.247	0.711 \pm 0.258	0.531 \pm 0.272	0.876 \pm 0.128
D=64	0.516 \pm 0.334	0.836 \pm 0.183	0.613 \pm 0.357	0.896 \pm 0.147	0.796 \pm 0.260	0.692 \pm 0.289	0.553 \pm 0.267	0.860 \pm 0.142
Horizon 25	0.502 \pm 0.328	0.854 \pm 0.150	0.599 \pm 0.361	0.907 \pm 0.118	0.821 \pm 0.250	0.676 \pm 0.294	0.517 \pm 0.304	0.881 \pm 0.128
Predict keys	0.405 \pm 0.332	0.735 \pm 0.233	0.495 \pm 0.369	0.803 \pm 0.227	0.748 \pm 0.312	0.622 \pm 0.359	0.462 \pm 0.279	0.857 \pm 0.126
Predict values	0.405 \pm 0.332	0.736 \pm 0.232	0.496 \pm 0.372	0.801 \pm 0.228	0.744 \pm 0.326	0.623 \pm 0.358	0.439 \pm 0.294	0.857 \pm 0.126
Predict attn map, Q	0.403 \pm 0.334	0.754 \pm 0.214	0.500 \pm 0.378	0.832 \pm 0.198	0.766 \pm 0.307	0.630 \pm 0.361	0.379 \pm 0.251	0.870 \pm 0.133
Predict attn map, QK	0.388 \pm 0.369	0.757 \pm 0.228	0.486 \pm 0.395	0.826 \pm 0.210	0.709 \pm 0.334	0.553 \pm 0.365	0.402 \pm 0.286	0.844 \pm 0.132
Predict hidden state	0.400 \pm 0.337	0.742 \pm 0.234	0.481 \pm 0.371	0.815 \pm 0.221	0.720 \pm 0.337	0.604 \pm 0.360	0.428 \pm 0.260	0.856 \pm 0.116

**Fig. 6.** Sensitivity to forecast horizon s (left) and tail aggregation length k (right) on the tuning subset.

Capacity and horizon. Reducing the number of attention heads from 8 to 4 (*Heads=4*) lowers AUC-PR by 0.033 with a smaller effect on localization metrics. Halving the model dimension from 128 to 64 (*D=64*) reduces AUC-PR by 0.042 and AUC-ROC by 0.025. Increasing the forecast horizon to $s = 25$ (*Horizon 25*) reduces AUC-PR by 0.056, consistent with a harder prediction task introducing more score variance at inference.

Prediction target. Predicting keys (*Predict keys*), values (*Predict values*), attention maps scored with query inputs only (*Predict attn map, Q*), attention maps scored with both query and key inputs (*Predict attn map, QK*), or intermediate hidden states (*Predict hidden state*) is consistently inferior to predicting query vectors across all ranking and localization metrics, supporting the design choice of query prediction as the supervision and scoring target.

Parameter sensitivity. Figure 6 shows sensitivity to the forecast horizon s and the tail length k . Performance peaks at $s = 1$ (AUC-PR 0.545, Range-F1

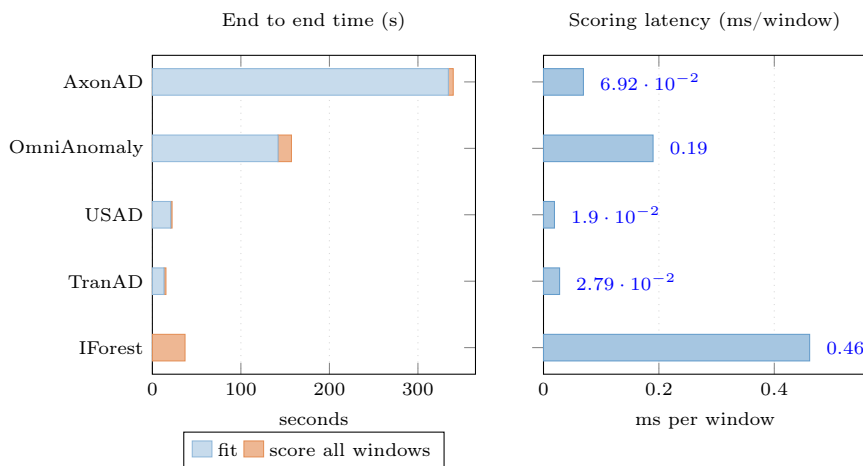


Fig. 7. Runtime on the telemetry stream (80,000 samples, stride 1). Left: wall-clock time split into fitting and scoring. Right: per window scoring latency. Classical baselines have no iterative training, so their time is entirely attributed to scoring.

0.553) and is generally lower for larger horizons, as a harder prediction task increases score variance. For tail length, threshold-free ranking is stable across $k \in \{3, 5, 10, 20\}$ (AUC-PR in $[0.524, 0.537]$), while Range-F1 peaks at $k = 10$, suggesting that k primarily controls temporal smoothing.

Mechanistic diagnostics. To verify that query mismatch captures meaningful attention structure rather than noise, we run a descriptive analysis on the tuning subset (not used for model selection). Spearman correlation between query deviation magnitude $\|\Delta Q\|$ and tail KL divergence $\text{KL}(A_{\text{tgt}} \| A_{\text{pred}})$, where A_{tgt} and A_{pred} denote attention weights from EMA target and predicted queries respectively, is frequently positive (median $\rho = 0.677$, $\rho \geq 0.50$ in 15 of 20 series). This confirms that query mismatch tracks genuine attention redistribution. Tail attention entropy is nondegenerate (range 3.18 to 4.53), ruling out collapsed attention as a confound.

The window-level correlation between reconstruction error and query mismatch is small (median $\rho = 0.211$). Among anomalous windows, the fraction with high query mismatch but low reconstruction error is 0.192, and the reverse is 0.095. Both regimes occur in most series, and combining components improves AUC-PR over the best single component in 8 of 20 series. This supports the coverage interpretation underlying the combined score.

Runtime. Figure 7 profiles runtime on the telemetry stream. AxonAD has the highest fitting cost (334s) but achieves per window scoring latency of 0.069 ms, lower than OmniAnomaly (0.190 ms) and Isolation Forest (0.461 ms). The fitting cost reflects iterative gradient-based training and is amortized at deployment. For a fleet monitoring pipeline processing windows at 10 Hz, the 0.069 ms latency leaves ample margin for real-time operation.

7 Conclusion

AxonAD detects multivariate time series anomalies by monitoring the predictability of attention query vectors. A bidirectional reconstruction pathway is coupled with a history-only predictor trained via masked EMA distillation in query space, producing a query mismatch signal that complements reconstruction residuals and responds to structural dependency shifts. Robust standardization of both components enables reliable score combination across heterogeneous datasets without label-based calibration.

On proprietary in-vehicle telemetry, where coordination breaks between steering, acceleration, and powertrain channels are the dominant fault mode, AxonAD improves AUC-PR by $2.2\times$ over the next best baseline and Event-F1 by $1.6\times$. These gains transfer to the multivariate TSB-AD benchmark (17 datasets, 180 series), where AxonAD leads on threshold-free ranking and range-aware localization. Ablations establish that query prediction outperforms alternative predictive targets and that combining both scores is necessary for the best aggregate performance. The low per window inference latency (0.069 ms) and the absence of label-based threshold tuning support integration into streaming vehicle monitoring pipelines.

References

1. Abrantes, J., Lange, R.T., Tang, Y.: Competition and Attraction Improve Model Fusion (Aug 2025). <https://doi.org/10.48550/arXiv.2508.16204>, <http://arxiv.org/abs/2508.16204>, arXiv:2508.16204
2. Assran, M., Duval, Q., Misra, I., Bojanowski, P., Vincent, P., Rabbat, M., LeCun, Y., Ballas, N.: Self-supervised learning from images with a joint-embedding predictive architecture. <https://doi.org/10.48550/arXiv.2301.08243>, <http://arxiv.org/abs/2301.08243>
3. Audibert, J., Michiardi, P., Guyard, F., Marti, S., Zuluaga, M.A.: USAD: UnSupervised anomaly detection on multivariate time series. In: Proceedings of the 26th ACM SIGKDD International Conference on Knowledge Discovery & Data Mining. pp. 3395–3404. ACM (2020). <https://doi.org/10.1145/3394486.3403392>, <https://dl.acm.org/doi/10.1145/3394486.3403392>
4. Ba, J.L., Kiros, J.R., Hinton, G.E.: Layer normalization (2016), <https://arxiv.org/abs/1607.06450>
5. Balestriero, R., LeCun, Y.: LeJEPa: Provable and scalable self-supervised learning without the heuristics. <https://doi.org/10.48550/arXiv.2511.08544>, <http://arxiv.org/abs/2511.08544>
6. Boniol, P., Krishna, A.K., Bruel, M., Liu, Q., Huang, M., Palpanas, T., Tsay, R.S., Elmore, A., Franklin, M.J., Paparrizos, J.: Vus: Effective and efficient accuracy measures for time-series anomaly detection (2025), <https://arxiv.org/abs/2502.13318>
7. Breunig, M.M., Kriegel, H.P., Ng, R.T., Sander, J.: LOF: identifying density-based local outliers **29**(2), 93–104 (2000). <https://doi.org/10.1145/335191.335388>, <https://dl.acm.org/doi/10.1145/335191.335388>

8. Candès, E.J., Li, X., Ma, Y., Wright, J.: Robust principal component analysis? **58**(3), 1–37 (2011). <https://doi.org/10.1145/1970392.1970395>, <https://dl.acm.org/doi/10.1145/1970392.1970395>
9. Cipolla, R., Gal, Y., Kendall, A.: Multi-task learning using uncertainty to weigh losses for scene geometry and semantics. In: 2018 IEEE/CVF Conference on Computer Vision and Pattern Recognition. pp. 7482–7491 (2018). <https://doi.org/10.1109/CVPR.2018.00781>
10. Correia, L., Goos, J.C., Klein, P., Bäck, T., Kononova, A.: MA-VAE: Multi-Head Attention-Based Variational Autoencoder Approach for Anomaly Detection in Multivariate Time-Series Applied to Automotive Endurance Powertrain Testing. In: Proceedings of the 15th International Joint Conference on Computational Intelligence. pp. 407–418. SCITEPRESS - Science and Technology Publications, Rome, Italy (2023). <https://doi.org/10.5220/0012163100003595>, <https://www.scitepress.org/DigitalLibrary/Link.aspx?doi=10.5220/0012163100003595>
11. Cover, T., Hart, P.: Nearest neighbor pattern classification. *IEEE Transactions on Information Theory* **13**(1), 21–27 (January 1967). <https://doi.org/10.1109/TIT.1967.1053964>
12. Deng, A., Hooi, B.: Graph Neural Network-Based Anomaly Detection in Multivariate Time Series (Jun 2021). <https://doi.org/10.48550/arXiv.2106.06947>, <http://arxiv.org/abs/2106.06947>, arXiv:2106.06947
13. Goldstein, M., Dengel, A.: Histogram-based outlier score (hbos): A fast unsupervised anomaly detection algorithm (09 2012)
14. Grill, J.B., Strub, F., Altché, F., Tallec, C., Richemond, P.H., Buchatskaya, E., Doersch, C., Pires, B.A., Guo, Z.D., Azar, M.G., Piot, B., Kavukcuoglu, K., Munos, R., Valko, M.: Bootstrap your own latent: A new approach to self-supervised learning (2020), <https://arxiv.org/abs/2006.07733>
15. Hariri, S., Kind, M.C., Brunner, R.J.: Extended Isolation Forest. *IEEE Transactions on Knowledge and Data Engineering* **33**(4), 1479–1489 (Apr 2021). <https://doi.org/10.1109/TKDE.2019.2947676>, <https://ieeexplore.ieee.org/document/8888179/>
16. He, Z., Xu, X., Deng, S.: Discovering cluster-based local outliers. *Pattern Recognition Letters* **24**(9), 1641–1650 (2003). [https://doi.org/https://doi.org/10.1016/S0167-8655\(03\)00003-5](https://doi.org/https://doi.org/10.1016/S0167-8655(03)00003-5), <https://www.sciencedirect.com/science/article/pii/S0167865503000035>
17. Lea, C., Flynn, M.D., Vidal, R., Reiter, A., Hager, G.D.: Temporal convolutional networks for action segmentation and detection. *CoRR* **abs/1611.05267** (2016), <http://arxiv.org/abs/1611.05267>
18. Li, L., Yan, J., Wang, H., Jin, Y.: Anomaly Detection of Time Series With Smoothness-Inducing Sequential Variational Auto-Encoder. *IEEE Transactions on Neural Networks and Learning Systems* **32**(3), 1177–1191 (Mar 2021). <https://doi.org/10.1109/TNNLS.2020.2980749>, <https://ieeexplore.ieee.org/document/9064715/>
19. Li, Z., Zhao, Y., Botta, N., Ionescu, C., Hu, X.: COPOD: Copula-based outlier detection. <https://doi.org/10.48550/arXiv.2009.09463>, <http://arxiv.org/abs/2009.09463>
20. Lim, B., Arık, S.Ö., Loeff, N., Pfister, T.: Temporal Fusion Transformers for interpretable multi-horizon time series forecasting. *International Journal of Forecasting* **37**(4), 1748–1764 (Oct 2021). <https://doi.org/10.1016/j.ijforecast.2021.03.012>, <https://www.sciencedirect.com/science/article/pii/S0169207021000637>

21. Liu, F.T., Ting, K.M., Zhou, Z.H.: Isolation Forest. In: 2008 Eighth IEEE International Conference on Data Mining. pp. 413–422 (Dec 2008). <https://doi.org/10.1109/ICDM.2008.17>, <https://ieeexplore.ieee.org/document/4781136>, ISSN: 2374-8486
22. Liu, Q., Paparrizos, J.: The Elephant in the Room: Towards A Reliable Time-Series Anomaly Detection Benchmark. In: Advances in Neural Information Processing Systems 37. pp. 108231–108261. Neural Information Processing Systems Foundation, Inc. (NeurIPS), Vancouver, BC, Canada (2024). <https://doi.org/10.52202/079017-3437>, <http://www.proceedings.com/079017-3437.html>
23. Loshchilov, I., Hutter, F.: Decoupled weight decay regularization (2019), <https://arxiv.org/abs/1711.05101>
24. Malhotra, P., Vig, L., Shroff, G., Agarwal, P.: Long short term memory networks for anomaly detection in time series (04 2015)
25. Paparrizos, J., Boniol, P., Palpanas, T., Tsay, R.S., Elmore, A., Franklin, M.J.: Volume under the surface: a new accuracy evaluation measure for time-series anomaly detection. *Proceedings of the VLDB Endowment* **15**(11), 2774–2787 (Jul 2022). <https://doi.org/10.14778/3551793.3551830>, <https://dl.acm.org/doi/10.14778/3551793.3551830>
26. Pereira, J., Silveira, M.: Unsupervised Anomaly Detection in Energy Time Series Data Using Variational Recurrent Autoencoders with Attention. In: 2018 17th IEEE International Conference on Machine Learning and Applications (ICMLA). pp. 1275–1282. IEEE, Orlando, FL (Dec 2018). <https://doi.org/10.1109/ICMLA.2018.00207>, <https://ieeexplore.ieee.org/document/8614232/>
27. Pereira, J., Silveira, M.: Unsupervised representation learning and anomaly detection in ECG sequences. *International Journal of Data Mining and Bioinformatics* **22**(4), 389 (2019). <https://doi.org/10.1504/IJDMB.2019.101395>, <http://www.inderscience.com/link.php?id=101395>
28. Su, Y., Zhao, Y., Niu, C., Liu, R., Sun, W., Pei, D.: Robust Anomaly Detection for Multivariate Time Series through Stochastic Recurrent Neural Network. In: Proceedings of the 25th ACM SIGKDD International Conference on Knowledge Discovery & Data Mining. pp. 2828–2837. ACM, Anchorage AK USA (Jul 2019). <https://doi.org/10.1145/3292500.3330672>, <https://dl.acm.org/doi/10.1145/3292500.3330672>
29. Tuli, S., Casale, G., Jennings, N.R.: TranAD: Deep Transformer Networks for Anomaly Detection in Multivariate Time Series Data (May 2022). <https://doi.org/10.48550/arXiv.2201.07284>, <http://arxiv.org/abs/2201.07284>, arXiv:2201.07284
30. Vaswani, A., Shazeer, N., Parmar, N., Uszkoreit, J., Jones, L., Gomez, A.N., Kaiser, L., Polosukhin, I.: Attention is all you need. In: Proceedings of the 31st International Conference on Neural Information Processing Systems. p. 6000–6010 (2017)
31. Von Schleinitz, J., Graf, M., Trutschnig, W., Schröder, A.: VASP: An autoencoder-based approach for multivariate anomaly detection and robust time series prediction with application in motorsport. *Engineering Applications of Artificial Intelligence* **104**, 104354 (Sep 2021). <https://doi.org/10.1016/j.engappai.2021.104354>, <https://linkinghub.elsevier.com/retrieve/pii/S0952197621002025>
32. Wu, H., Hu, T., Liu, Y., Zhou, H., Wang, J., Long, M.: TimesNet: Temporal 2D-Variation Modeling for General Time Series Analysis (Apr 2023). <https://doi.org/10.48550/arXiv.2210.02186>, <http://arxiv.org/abs/2210.02186>, arXiv:2210.02186

33. Xu, H., Chen, W., Zhao, N., Li, Z., Bu, J., Li, Z., Liu, Y., Zhao, Y., Pei, D., Feng, Y., Chen, J., Wang, Z., Qiao, H.: Unsupervised Anomaly Detection via Variational Auto-Encoder for Seasonal KPIs in Web Applications (Feb 2018). <https://doi.org/10.48550/arXiv.1802.03903>, <http://arxiv.org/abs/1802.03903>, arXiv:1802.03903
34. Xu, J., Wu, H., Wang, J., Long, M.: Anomaly Transformer: Time Series Anomaly Detection with Association Discrepancy (Jun 2022). <https://doi.org/10.48550/arXiv.2110.02642>, <http://arxiv.org/abs/2110.02642>, arXiv:2110.02642
35. Xu, Z., Zeng, A., Xu, Q.: FITS: Modeling time series with 10^k parameters. <https://doi.org/10.48550/arXiv.2307.03756>, <http://arxiv.org/abs/2307.03756>
36. Yairi, T., Kato, Y., Hori, K.: Fault detection by mining association rules from housekeeping data (06 2001)
37. Zhou, T., Niu, P., Wang, X., Sun, L., Jin, R.: One fits all: power general time series analysis by pretrained lm (2023), <https://arxiv.org/abs/2302.11939>

Predictable Query Dynamics for Time-Series Anomaly Detection

Supplementary Material

1 Additional Tables

Table 1. TSB-AD multivariate benchmark (17 datasets, 180 time series). Mean \pm standard deviation over all evaluated series. Best result per metric in **bold**.

Model	TSB-AD (multivariate, 17 datasets, 180 time series)							
	AUC-PR	AUC-ROC	VUS-PR	VUS-ROC	PA-F1	Event-F1	Range-F1	Affiliation-F1
VASP	0.339 \pm 0.319	0.762 \pm 0.195	0.401 \pm 0.338	0.809 \pm 0.185	0.669 \pm 0.318	0.520 \pm 0.361	0.400 \pm 0.260	0.849 \pm 0.123
OmniAnomaly	0.372 \pm 0.341	0.744 \pm 0.250	0.424 \pm 0.354	0.777 \pm 0.240	0.627 \pm 0.354	0.528 \pm 0.367	0.432 \pm 0.292	0.841 \pm 0.126
WVAE	0.354 \pm 0.331	0.747 \pm 0.248	0.413 \pm 0.349	0.778 \pm 0.248	0.576 \pm 0.388	0.502 \pm 0.383	0.365 \pm 0.280	0.838 \pm 0.137
USAD	0.363 \pm 0.339	0.738 \pm 0.256	0.412 \pm 0.350	0.771 \pm 0.244	0.622 \pm 0.355	0.519 \pm 0.364	0.422 \pm 0.288	0.837 \pm 0.131
SISVAE	0.323 \pm 0.290	0.759 \pm 0.234	0.372 \pm 0.315	0.786 \pm 0.227	0.551 \pm 0.367	0.470 \pm 0.355	0.369 \pm 0.278	0.824 \pm 0.129
OFA	0.300 \pm 0.300	0.639 \pm 0.289	0.367 \pm 0.342	0.694 \pm 0.286	0.675 \pm 0.305	0.517 \pm 0.372	0.360 \pm 0.251	0.833 \pm 0.126
CNN	0.347 \pm 0.356	0.770 \pm 0.176	0.352 \pm 0.359	0.807 \pm 0.164	0.828 \pm 0.266	0.643 \pm 0.366	0.301 \pm 0.240	0.866 \pm 0.120
MAVAE	0.299 \pm 0.297	0.697 \pm 0.256	0.351 \pm 0.322	0.728 \pm 0.256	0.568 \pm 0.372	0.463 \pm 0.360	0.325 \pm 0.264	0.812 \pm 0.132
VSVAE	0.290 \pm 0.286	0.709 \pm 0.256	0.342 \pm 0.321	0.734 \pm 0.257	0.596 \pm 0.355	0.487 \pm 0.347	0.374 \pm 0.254	0.841 \pm 0.121
GDN	0.272 \pm 0.305	0.738 \pm 0.193	0.332 \pm 0.329	0.802 \pm 0.175	0.756 \pm 0.310	0.499 \pm 0.364	0.208 \pm 0.134	0.846 \pm 0.119
M2N2	0.319 \pm 0.358	0.740 \pm 0.198	0.323 \pm 0.359	0.779 \pm 0.183	0.876 \pm 0.184	0.603 \pm 0.372	0.282 \pm 0.233	0.860 \pm 0.118
TranAD	0.258 \pm 0.318	0.675 \pm 0.221	0.308 \pm 0.347	0.742 \pm 0.210	0.753 \pm 0.314	0.530 \pm 0.367	0.218 \pm 0.154	0.826 \pm 0.125
TFTResidual	0.250 \pm 0.313	0.710 \pm 0.210	0.308 \pm 0.338	0.777 \pm 0.186	0.746 \pm 0.318	0.472 \pm 0.362	0.207 \pm 0.161	0.846 \pm 0.114
KMeansAD	0.252 \pm 0.267	0.691 \pm 0.202	0.296 \pm 0.302	0.732 \pm 0.195	0.675 \pm 0.309	0.483 \pm 0.364	0.326 \pm 0.235	0.819 \pm 0.126
AutoEncoder	0.294 \pm 0.373	0.669 \pm 0.212	0.295 \pm 0.368	0.691 \pm 0.207	0.597 \pm 0.357	0.439 \pm 0.411	0.283 \pm 0.297	0.800 \pm 0.139
PCA	0.242 \pm 0.293	0.676 \pm 0.238	0.277 \pm 0.307	0.712 \pm 0.223	0.514 \pm 0.340	0.370 \pm 0.329	0.325 \pm 0.263	0.789 \pm 0.122
TimesNet	0.201 \pm 0.246	0.618 \pm 0.279	0.271 \pm 0.297	0.686 \pm 0.277	0.750 \pm 0.292	0.427 \pm 0.354	0.176 \pm 0.129	0.821 \pm 0.117
FITS	0.197 \pm 0.253	0.611 \pm 0.271	0.267 \pm 0.300	0.686 \pm 0.274	0.763 \pm 0.281	0.422 \pm 0.342	0.181 \pm 0.131	0.816 \pm 0.115
Donut	0.213 \pm 0.270	0.627 \pm 0.239	0.262 \pm 0.308	0.693 \pm 0.237	0.525 \pm 0.414	0.406 \pm 0.385	0.180 \pm 0.167	0.769 \pm 0.200
CBLOF	0.263 \pm 0.344	0.664 \pm 0.206	0.260 \pm 0.341	0.697 \pm 0.193	0.648 \pm 0.340	0.448 \pm 0.412	0.302 \pm 0.283	0.811 \pm 0.149
IForest	0.210 \pm 0.232	0.704 \pm 0.191	0.253 \pm 0.260	0.750 \pm 0.184	0.655 \pm 0.335	0.403 \pm 0.322	0.243 \pm 0.178	0.801 \pm 0.110
LSTMAD	0.248 \pm 0.328	0.597 \pm 0.337	0.245 \pm 0.329	0.626 \pm 0.343	0.657 \pm 0.412	0.507 \pm 0.413	0.198 \pm 0.175	0.701 \pm 0.350
RobustPCA	0.238 \pm 0.349	0.589 \pm 0.241	0.238 \pm 0.352	0.616 \pm 0.235	0.573 \pm 0.387	0.379 \pm 0.385	0.332 \pm 0.318	0.789 \pm 0.135
EIF	0.186 \pm 0.218	0.667 \pm 0.174	0.210 \pm 0.258	0.708 \pm 0.168	0.741 \pm 0.291	0.438 \pm 0.374	0.258 \pm 0.230	0.812 \pm 0.121
COPOD	0.205 \pm 0.292	0.652 \pm 0.185	0.203 \pm 0.290	0.686 \pm 0.177	0.717 \pm 0.320	0.414 \pm 0.364	0.242 \pm 0.237	0.799 \pm 0.128
HBOS	0.161 \pm 0.196	0.633 \pm 0.183	0.190 \pm 0.247	0.672 \pm 0.184	0.667 \pm 0.331	0.399 \pm 0.345	0.244 \pm 0.225	0.796 \pm 0.117
KNN	0.133 \pm 0.156	0.499 \pm 0.218	0.176 \pm 0.220	0.580 \pm 0.219	0.681 \pm 0.366	0.447 \pm 0.391	0.205 \pm 0.149	0.791 \pm 0.140
LOF	0.096 \pm 0.092	0.534 \pm 0.098	0.138 \pm 0.192	0.597 \pm 0.147	0.563 \pm 0.368	0.325 \pm 0.328	0.149 \pm 0.143	0.764 \pm 0.133
AnomalyTransformer	0.068 \pm 0.060	0.506 \pm 0.053	0.115 \pm 0.184	0.538 \pm 0.098	0.658 \pm 0.359	0.361 \pm 0.363	0.138 \pm 0.121	0.737 \pm 0.195
AxonAD (ours)	0.437 \pm 0.323	0.825 \pm 0.169	0.493 \pm 0.325	0.859 \pm 0.146	0.698 \pm 0.316	0.600 \pm 0.336	0.471 \pm 0.290	0.860 \pm 0.132

Table 2. TSB-AD multivariate benchmark protocol on proprietary dataset. Mean \pm standard deviation over 4 random seeds. Best result per metric in **bold**.

Model	TSB-AD (Proprietary Dataset)							
	AUC-PR	AUC-ROC	VUS-PR	VUS-ROC	PA-F1	Event-F1	Range-F1	Affiliation-F1
LSTMAD	0.082 \pm 0.004	0.651 \pm 0.009	0.083 \pm 0.004	0.624 \pm 0.009	0.533 \pm 0.014	0.255 \pm 0.015	0.139 \pm 0.006	0.723 \pm 0.003
SISVAE	0.128 \pm 0.030	0.586 \pm 0.026	0.070 \pm 0.012	0.504 \pm 0.052	0.270 \pm 0.100	0.231 \pm 0.060	0.225 \pm 0.054	0.699 \pm 0.018
TFTRResidual	0.071 \pm 0.006	0.644 \pm 0.025	0.070 \pm 0.005	0.582 \pm 0.018	0.424 \pm 0.022	0.164 \pm 0.019	0.110 \pm 0.009	0.752 \pm 0.026
RobustPCA	0.070 \pm 0.000	0.634 \pm 0.000	0.066 \pm 0.000	0.570 \pm 0.000	0.312 \pm 0.000	0.162 \pm 0.000	0.100 \pm 0.000	0.680 \pm 0.000
VSSVAE	0.100 \pm 0.005	0.617 \pm 0.031	0.065 \pm 0.005	0.535 \pm 0.027	0.214 \pm 0.048	0.188 \pm 0.004	0.262 \pm 0.037	0.730 \pm 0.012
M2N2	0.065 \pm 0.001	0.596 \pm 0.001	0.064 \pm 0.001	0.553 \pm 0.004	0.392 \pm 0.022	0.196 \pm 0.020	0.120 \pm 0.009	0.680 \pm 0.000
OFA	0.061 \pm 0.002	0.597 \pm 0.003	0.060 \pm 0.001	0.542 \pm 0.001	0.224 \pm 0.010	0.109 \pm 0.007	0.122 \pm 0.015	0.680 \pm 0.000
MAVAE	0.094 \pm 0.006	0.561 \pm 0.034	0.059 \pm 0.006	0.487 \pm 0.051	0.220 \pm 0.076	0.199 \pm 0.015	0.202 \pm 0.017	0.680 \pm 0.000
KNN	0.085 \pm 0.000	0.563 \pm 0.000	0.059 \pm 0.000	0.506 \pm 0.000	0.336 \pm 0.000	0.231 \pm 0.000	0.080 \pm 0.000	0.680 \pm 0.000
CNN	0.058 \pm 0.002	0.568 \pm 0.006	0.059 \pm 0.002	0.524 \pm 0.007	0.382 \pm 0.033	0.186 \pm 0.018	0.105 \pm 0.004	0.681 \pm 0.003
WVAE	0.087 \pm 0.013	0.541 \pm 0.043	0.057 \pm 0.007	0.467 \pm 0.050	0.249 \pm 0.103	0.226 \pm 0.038	0.163 \pm 0.011	0.680 \pm 0.000
LOF	0.055 \pm 0.000	0.543 \pm 0.000	0.056 \pm 0.000	0.552 \pm 0.000	0.561 \pm 0.000	0.166 \pm 0.000	0.124 \pm 0.000	0.680 \pm 0.000
TimesNet	0.055 \pm 0.001	0.579 \pm 0.003	0.056 \pm 0.000	0.531 \pm 0.003	0.306 \pm 0.020	0.102 \pm 0.004	0.092 \pm 0.002	0.680 \pm 0.000
FITS	0.050 \pm 0.000	0.563 \pm 0.000	0.053 \pm 0.000	0.548 \pm 0.001	0.451 \pm 0.002	0.091 \pm 0.001	0.071 \pm 0.001	0.680 \pm 0.000
GDN	0.052 \pm 0.006	0.547 \pm 0.027	0.052 \pm 0.004	0.478 \pm 0.027	0.349 \pm 0.074	0.115 \pm 0.028	0.087 \pm 0.005	0.681 \pm 0.004
VASP	0.050 \pm 0.001	0.540 \pm 0.014	0.051 \pm 0.002	0.449 \pm 0.016	0.190 \pm 0.008	0.099 \pm 0.004	0.119 \pm 0.013	0.686 \pm 0.008
AutoEncoder	0.047 \pm 0.003	0.541 \pm 0.018	0.051 \pm 0.003	0.495 \pm 0.022	0.185 \pm 0.026	0.107 \pm 0.005	0.084 \pm 0.016	0.680 \pm 0.000
EIF	0.049 \pm 0.002	0.500 \pm 0.006	0.047 \pm 0.000	0.357 \pm 0.010	0.224 \pm 0.019	0.118 \pm 0.014	0.192 \pm 0.016	0.690 \pm 0.007
AnomalyTransformer	0.045 \pm 0.003	0.491 \pm 0.019	0.047 \pm 0.002	0.454 \pm 0.032	0.379 \pm 0.031	0.118 \pm 0.033	0.064 \pm 0.006	0.591 \pm 0.086
HBOS	0.064 \pm 0.000	0.479 \pm 0.000	0.046 \pm 0.000	0.349 \pm 0.000	0.282 \pm 0.000	0.171 \pm 0.000	0.193 \pm 0.000	0.701 \pm 0.000
KMeansAD	0.042 \pm 0.000	0.495 \pm 0.000	0.046 \pm 0.000	0.343 \pm 0.000	0.161 \pm 0.009	0.087 \pm 0.002	0.098 \pm 0.007	0.680 \pm 0.000
CBLOF	0.041 \pm 0.000	0.481 \pm 0.000	0.044 \pm 0.000	0.352 \pm 0.000	0.155 \pm 0.000	0.086 \pm 0.000	0.073 \pm 0.000	0.680 \pm 0.000
IForest	0.041 \pm 0.000	0.472 \pm 0.000	0.044 \pm 0.000	0.328 \pm 0.000	0.140 \pm 0.000	0.086 \pm 0.000	0.195 \pm 0.000	0.682 \pm 0.000
TranAD	0.041 \pm 0.000	0.470 \pm 0.003	0.044 \pm 0.000	0.417 \pm 0.004	0.237 \pm 0.003	0.086 \pm 0.000	0.107 \pm 0.007	0.680 \pm 0.000
USAD	0.040 \pm 0.001	0.470 \pm 0.010	0.044 \pm 0.001	0.371 \pm 0.011	0.122 \pm 0.005	0.087 \pm 0.001	0.152 \pm 0.033	0.682 \pm 0.001
PCA	0.037 \pm 0.000	0.447 \pm 0.000	0.043 \pm 0.000	0.377 \pm 0.000	0.107 \pm 0.000	0.092 \pm 0.000	0.148 \pm 0.000	0.684 \pm 0.000
OmniAnomaly	0.041 \pm 0.000	0.459 \pm 0.000	0.043 \pm 0.000	0.338 \pm 0.000	0.150 \pm 0.000	0.086 \pm 0.000	0.126 \pm 0.000	0.680 \pm 0.000
COPOD	0.035 \pm 0.000	0.433 \pm 0.000	0.041 \pm 0.000	0.368 \pm 0.000	0.131 \pm 0.000	0.090 \pm 0.000	0.170 \pm 0.000	0.710 \pm 0.000
Donut	0.036 \pm 0.001	0.443 \pm 0.020	0.041 \pm 0.001	0.386 \pm 0.027	0.091 \pm 0.006	0.086 \pm 0.000	0.098 \pm 0.059	0.680 \pm 0.000
AxonAD (ours)	0.285 \pm 0.014	0.702 \pm 0.011	0.157 \pm 0.012	0.634 \pm 0.017	0.533 \pm 0.016	0.420 \pm 0.019	0.328 \pm 0.014	0.715 \pm 0.024

Table 3. Pairwise comparison against **AxonAD** on TSB-AD multivariate (17 datasets, 180 time series). For each baseline and metric we report: win-rate (wins/180), mean and median performance delta (Δ), Wilcoxon p -value, and 95% CI for Δ . Negative Δ indicates the baseline is worse than AxonAD (per your export). Entries with non-significant Wilcoxon test ($p \geq 0.05$) are **bold**.

Model	AUC-PR (vs AxonAD)					AUC-ROC (vs AxonAD)						
	WR	Δ	mean Δ	med	p	CI_{95}	WR	Δ	mean Δ	med	p	CI_{95}
AnomalyTransformer	0.039	-0.3693	-0.3203	1.24×10^{-30}	0.033	[-0.4124, -0.3255]	0.033	-0.3185	-0.3520	1.14×10^{-29}	0.033	[-0.3432, -0.2919]
AutoEncoder	0.194	-0.1427	-0.1462	1.93×10^{-11}	0.172	[-0.1969, -0.0882]	0.172	-0.1554	-0.1776	2.33×10^{-14}	0.172	[-0.1916, -0.1224]
CBLOF	0.178	-0.1738	-0.1506	2.19×10^{-13}	0.139	[-0.2287, -0.1185]	0.139	-0.1610	-0.1601	6.06×10^{-16}	0.139	[-0.1949, -0.1268]
CNN	0.267	-0.0899	-0.0859	1.36×10^{-8}	0.228	[-0.1388, -0.0393]	0.228	-0.0544	-0.0555	2.24×10^{-8}	0.228	[-0.0829, -0.0268]
COPOD	0.194	-0.2324	-0.2315	2.30×10^{-14}	0.133	[-0.2903, -0.1716]	0.133	-0.1730	-0.2094	2.19×10^{-16}	0.133	[-0.2064, -0.1398]
Domut	0.117	-0.2237	-0.1705	2.11×10^{-22}	0.122	[-0.2635, -0.1844]	0.122	-0.1978	-0.1527	6.15×10^{-23}	0.122	[-0.2329, -0.1657]
EIF	0.189	-0.2505	-0.2159	1.98×10^{-17}	0.150	[-0.2998, -0.2029]	0.150	-0.1582	-0.1657	1.57×10^{-16}	0.150	[-0.1888, -0.1277]
FITS	0.061	-0.2398	-0.1988	2.99×10^{-28}	0.094	[-0.2730, -0.2076]	0.094	-0.2138	-0.1651	5.35×10^{-25}	0.094	[-0.2496, -0.1779]
GDN	0.156	-0.1647	-0.1067	1.01×10^{-20}	0.189	[-0.1964, -0.1345]	0.189	-0.0870	-0.0667	4.46×10^{-14}	0.189	[-0.1108, -0.0643]
HBOS	0.194	-0.2759	-0.2588	2.24×10^{-19}	0.128	[-0.3224, -0.2293]	0.128	-0.1916	-0.1984	2.23×10^{-20}	0.128	[-0.2217, -0.1611]
IForest	0.217	-0.2274	-0.1814	5.74×10^{-15}	0.200	[-0.2780, -0.1776]	0.200	-0.1207	-0.1122	5.24×10^{-15}	0.200	[-0.1503, -0.0908]
KMeansAD	0.239	-0.1853	-0.1482	4.22×10^{-12}	0.261	[-0.2335, -0.1336]	0.261	-0.1337	-0.1174	3.58×10^{-14}	0.261	[-0.1646, -0.1023]
KNN	0.128	-0.3043	-0.2596	1.09×10^{-25}	0.039	[-0.3452, -0.2632]	0.039	-0.3257	-0.3305	1.04×10^{-29}	0.039	[-0.3554, -0.2940]
LOF	0.133	-0.3406	-0.2886	2.50×10^{-25}	0.039	[-0.3881, -0.2962]	0.039	-0.2906	-0.3184	7.00×10^{-30}	0.039	[-0.3126, -0.2674]
LSTMAD	0.144	-0.1893	-0.1256	9.95×10^{-21}	0.139	[-0.2249, -0.1550]	0.139	-0.2274	-0.1489	3.90×10^{-22}	0.139	[-0.2673, -0.1873]
M2N2	0.239	-0.1181	-0.0955	3.82×10^{-10}	0.217	[-0.1695, -0.0663]	0.217	-0.0851	-0.0866	2.90×10^{-10}	0.217	[-0.1162, -0.0542]
MAVAE	0.322	-0.1380	-0.0390	2.07×10^{-9}	0.317	[-0.1802, -0.0936]	0.317	-0.1273	-0.0279	6.14×10^{-10}	0.317	[-0.1621, -0.0932]
OFA	0.217	-0.1368	-0.0907	1.09×10^{-15}	0.206	[-0.1715, -0.1029]	0.206	-0.1855	-0.1181	1.35×10^{-16}	0.206	[-0.2228, -0.1473]
OmniAnomaly	0.328	-0.0649	-0.0190	2.76×10^{-5}	0.372	[-0.0961, -0.0354]	0.372	-0.0806	-0.0043	1.94×10^{-5}	0.372	[-0.1097, -0.0518]
PCA	0.161	-0.1949	-0.1406	1.09×10^{-15}	0.178	[-0.2428, -0.1483]	0.178	-0.1488	-0.0990	2.65×10^{-19}	0.178	[-0.1793, -0.1211]
RobustPCA	0.150	-0.1989	-0.2100	1.05×10^{-15}	0.106	[-0.2548, -0.1407]	0.106	-0.2354	-0.2480	3.91×10^{-19}	0.106	[-0.2782, -0.1953]
SISVAE	0.272	-0.1143	-0.0522	1.73×10^{-11}	0.322	[-0.1511, -0.0781]	0.322	-0.0659	-0.0157	9.74×10^{-7}	0.322	[-0.0917, -0.0403]
TFTResidual	0.133	-0.1868	-0.1252	4.79×10^{-21}	0.206	[-0.2212, -0.1509]	0.206	-0.1152	-0.0852	1.54×10^{-14}	0.206	[-0.1429, -0.0886]
TimesNet	0.117	-0.2355	-0.1916	5.03×10^{-27}	0.133	[-0.2693, -0.2038]	0.133	-0.2068	-0.1294	1.99×10^{-22}	0.133	[-0.2433, -0.1702]
TranAD	0.194	-0.1793	-0.1080	1.24×10^{-18}	0.161	[-0.2153, -0.1433]	0.161	-0.1498	-0.1024	5.06×10^{-19}	0.161	[-0.1791, -0.1197]
USAD	0.294	-0.0744	-0.0275	2.14×10^{-7}	0.294	[-0.1044, -0.0451]	0.294	-0.0867	-0.0084	2.33×10^{-8}	0.294	[-0.1159, -0.0580]
VASP	0.289	-0.0978	-0.0449	1.83×10^{-10}	0.333	[-0.1286, -0.0676]	0.333	-0.0626	-0.0158	1.13×10^{-6}	0.333	[-0.0857, -0.0400]
VSAE	0.333	-0.1465	-0.0592	8.43×10^{-9}	0.378	[-0.1927, -0.1017]	0.378	-0.1159	-0.0281	1.17×10^{-6}	0.378	[-0.1525, -0.0778]
WVAE	0.322	-0.0829	-0.0381	5.57×10^{-7}	0.372	[-0.1182, -0.0451]	0.372	-0.0775	-0.0103	8.81×10^{-5}	0.372	[-0.1086, -0.0479]

Table 4. Continuation of Table 3: VUS-PR, R-based-F1, and Affiliation-F1 vs AxonAD. Missing metrics in your export (VUS-ROC, PA-F1, Event-F1, Range-F1) are not shown.

Model	VUS-PR (vs AxonAD)					R-based-F1 (vs AxonAD)					Affiliation-F (vs AxonAD)							
	WR	Δ	mean Δ	med	p	CI_{95}	WR	Δ	mean Δ	med	p	CI_{95}	WR	Δ	mean Δ	med	p	CI_{95}
AnomalyTransformer	0.039	-0.3784	-0.2998	1.65×10^{-30}	0.067	[-0.4217, -0.3367]	0.067	-0.3325	-0.3168	2.57×10^{-29}	0.200	[-0.3678, -0.2964]	0.200	-0.1228	-0.0718	3.64×10^{-18}	0.039	[-0.1478, -0.0993]
AutoEncoder	0.172	-0.1987	-0.1348	1.88×10^{-16}	0.189	[-0.2422, -0.1567]	0.189	-0.1882	-0.2248	2.51×10^{-13}	0.333	[-0.2396, -0.1352]	0.333	-0.0596	-0.0207	6.96×10^{-7}	0.172	[-0.0831, -0.0354]
CBLOF	0.161	-0.2334	-0.1601	1.49×10^{-19}	0.200	[-0.2776, -0.1924]	0.200	-0.1692	-0.2151	1.54×10^{-12}	0.361	[-0.2177, -0.1185]	0.361	-0.0487	-0.0081	8.71×10^{-5}	0.161	[-0.0752, -0.0225]
CNN	0.278	-0.1408	-0.0769	9.59×10^{-12}	0.217	[-0.1805, -0.1039]	0.217	-0.1694	-0.1844	3.38×10^{-13}	0.483	[-0.2190, -0.1180]	0.483	0.0062	-0.0002	0.676	0.278	[-0.0127, -0.0264]
COPOD	0.150	-0.2900	-0.2262	3.03×10^{-22}	0.183	[-0.3360, -0.2450]	0.183	-0.2287	-0.2535	6.43×10^{-15}	0.333	[-0.2815, -0.1741]	0.333	-0.0609	-0.0538	2.21×10^{-7}	0.150	[-0.0853, -0.0363]
Domut	0.100	-0.2312	-0.1677	2.85×10^{-22}	0.100	[-0.2700, -0.1925]	0.100	-0.2913	-0.2873	7.64×10^{-27}	0.261	[-0.3273, -0.2543]	0.261	-0.0913	-0.0147	1.59×10^{-13}	0.100	[-0.1181, -0.0681]
EIF	0.161	-0.2836	-0.1920	2.10×10^{-23}	0.189	[-0.3275, -0.2431]	0.189	-0.2125	-0.2535	3.91×10^{-14}	0.367	[-0.2640, -0.1614]	0.367	-0.0477	-0.0163	1.59×10^{-6}	0.161	[-0.0704, -0.0255]
FITS	0.100	-0.2265	-0.1607	1.92×10^{-26}	0.261	[-0.2615, -0.1927]	0.261	-0.2898	-0.2569	9.49×10^{-27}	0.439	[-0.3269, -0.2536]	0.439	-0.0445	-0.0226	1.56×10^{-7}	0.100	[-0.0668, -0.0286]
GDN	0.161	-0.1611	-0.0866	1.87×10^{-19}	0.111	[-0.1936, -0.1294]	0.111	-0.2625	-0.2455	1.79×10^{-25}	0.372	[-0.2969, -0.2273]	0.372	-0.0145	-0.0024	0.0621	0.161	[-0.0308, 0.0024]
HBOS	0.128	-0.3030	-0.2395	9.54×10^{-25}	0.189	[-0.3484, -0.2584]	0.189	-0.2271	-0.2438	7.61×10^{-15}	0.333	[-0.2803, -0.1770]	0.333	-0.0637	-0.0600	3.80×10^{-8}	0.128	[-0.0855, -0.0419]
IForest	0.189	-0.2399	-0.2016	8.52×10^{-17}	0.217	[-0.2862, -0.1896]	0.217	-0.2275	-0.2268	9.05×10^{-18}	0.339	[-0.2689, -0.1849]	0.339	-0.0590	-0.0399	4.68×10^{-9}	0.189	[-0.0767, -0.0401]
KMeansAD	0.239	-0.1970	-0.1592	2.18×10^{-14}	0.289	[-0.2403, -0.1514]	0.289	-0.1449	-0.1326	1.06×10^{-8}	0.422	[-0.1866, -0.0998]	0.422	-0.0407	-0.0138	1.06×10^{-4}	0.239	[-0.0599, -0.0196]
KNN	0.061	-0.3168	-0.2638	1.46×10^{-28}	0.167	[-0.3565, -0.2764]	0.167	-0.2660	-0.2216	6.33×10^{-23}	0.300	[-0.3040, -0.2264]	0.300	-0.0695	-0.0435	2.44×10^{-9}	0.061	[-0.0909, -0.0484]
LOF	0.067	-0.3548	-0.2799	2.79×10^{-29}	0.133	[-0.3986, -0.3115]	0.133	-0.3220	-0.2865	1.54×10^{-25}	0.279	[-0.3641, -0.2781]	0.279	-0.0953	-0.0677	9.44×10^{-12}	0.067	[-0.1179, -0.0716]
LSTMAD	0.144	-0.2482	-0.1504	8.26×10^{-22}	0.094	[-0.2914, -0.2049]	0.094	-0.2726	-0.2264	1.95×10^{-27}	0.344	[-0.3066, -0.2361]	0.344	-0.1594	-0.0079	6.26×10^{-8}	0.144	[-0.2043, -0.1159]
M2N2	0.228	-0.1702	-0.0953	5.15×10^{-14}	0.206	[-0.2105, -0.1322]	0.206	-0.1889	-0.2161	3.35×10^{-14}	0.439	[-0.2381, -0.1375]	0.439	-0.0004	-0.0011	0.376	0.228	[-0.0183, 0.0175]
MAVAE	0.300	-0.1425	-0.0495	2.12×10^{-10}	0.228	[-0.1839, -0.0997]	0.228	-0.1455	-0.0838	1.20×10^{-15}	0.322	[-0.1805, -0.1105]	0.322	-0.0484	-0.0026	4.08×10^{-8}	0.300	[-0.0648, -0.0310]
OFA	0.222	-0.1260	-0.0797	3.25×10^{-14}	0.283	[-0.1600, -0.0930]	0.283	-0.1111	-0.0820	4.37×10^{-11}	0.367	[-0.1419, -0.0796]	0.367	-0.0275	-0.0035	7.76×10^{-4}	0.222	[-0.0429, -0.0124]
OmniAnomaly	0.328	-0.0697	-0.0172	6.67×10^{-6}	0.361	[-0.0998, -0.0396]	0.361	-0.0393	-0.0153	3.44×10^{-3}	0.422	[-0.0691, -0.0107]	0.422	-0.0186	-0.0002	0.0852	0.328	[-0.0358, -0.0010]
PCA	0.161	-0.2167	-0.1472	2.20×10^{-18}	0.267	[-0.2611, -0.1722]	0.267	-0.1456	-0.0754	3.45×10^{-11								